Characteristics of total gaseous mercury (TGM) concentrations in an industrial complex in southern Korea: Impacts from local sources

Yong-Seok Seo[1,2], Seung-Pyo Jeong[1], Thomas M. Holsen[3], Young-Ji Han[4], Eunhwa Choi[5], Eun Ha Park[1], Tae Young Kim[1], Hee-Sang Eum[1], Dae Gun Park[1], Eunhye Kim[6], Soontae Kim[6], Jeong-Hun Kim[7], Jaewon Choi[8], Seung-Muk Yi[1,2,*]

[1]Department of Environmental Health, Graduate School of Public Health, Seoul National University, 1 Gwanak, Gwanak-ro, Gwanak-gu, Seoul 151-742, South Korea

[2]Institute of Health and Environment, Seoul National University, 1 Gwanak, Gwanak-ro, Gwanak-gu, Seoul 151-742, South Korea

[3]Department of Civil and Environmental Engineering, Clarkson University, Potsdam, NY13699, USA

[4]Department of Environmental Science, Kangwon National University, 192-1, Hyoja-2-dong, Chuncheon, Kangwondo, 200-701, South Korea

[5]Asian Institute for Energy, Environment & Sustainability, Seoul National University, 1 Gwanak-ro, Gwanak-gu, Seoul 151-742, South Korea

[6]Department of Environmental, Civil and Transportation Engineering, Ajou University, Woncheon-dong, Yeongtong-gu, Suwon, 443-749, South Korea

[7]Division of Air Pollution Engineering, Department of Climate and Air Quality Research, National Institute of Environmental Research, Hwangyong-ro 42, Seogu, Incheon, 404-708, South Korea

[8]University of Pennsylvania, Philadelphia, PA19104, USA

[*]Address correspondence to Dr. Seung-Muk Yi, Graduate School of Public Health, Seoul National University, 1 Gwanak, Gwanak-ro, Gwanak-gu, Seoul 151-742, South Korea
E-mail) yiseung@snu.ac.kr
Telephone) 82-2-880-2736
Fax) 82-2-745-9104

45 **Abstract**

46   Total gaseous mercury (TGM) concentrations were measured every 5 min in Pohang,

47 Gyeongsangbuk-do, Korea during summer (17 August~23 August 2012), fall (9 October~17

48 October 2012), winter (22 January ~29 January 2013), and spring (26 March~3 April 2013)

49 to: 1) characterize the hourly and seasonal variations of atmospheric TGM concentrations, 2)

50 identify the relationships between TGM and co-pollutants, and 3) identify likely source

51 directions and locations of TGM using conditional probability function (CPF), conditional

52 bivariate probability function (CBPF) and total potential source contribution function

53 (TPSCF).

54   The TGM concentration was statistically significantly highest in fall (6.7 ± 6.4 ng m^{-3}),

55 followed by spring (4.8 ± 4.0 ng m^{-3}), winter (4.5 ± 3.2 ng m^{-3}) and summer (3.8 ± 3.9 ng m^{-}

56 ^{3}). There was a weak but statistically significant negative correlation between the TGM

57 concentration and ambient air temperature *(r = -0.08) (p < 0.05).* Although the daytime

58 temperature (14.7 ± 10.0 ℃) was statistically significantly higher than that in the nighttime

59 (13.0 ± 9.8 ℃) ($p < 0.05$), the daytime TGM concentration (5.3 ± 4.7 ng m^{-3}) was statistically

60 significantly higher than those in the nighttime (4.7 ± 4.7 ng m^{-3}) ($p < 0.01$), possibly due to

61 local emissions related to industrial activities and activation of local surface emission

62 sources. The observed ΔTGM/ΔCO was significantly lower than that of Asian long-range

63 transport, but similar to that of local sources in Korea and in US industrial events suggesting

64 that local sources are more important than that of long-range transport. CPF, CBPF and

65 TPSCF indicated that the main sources of TGM were iron and manufacturing facilities, the

66 hazardous waste incinerators and the coastal areas.

67   **Keywords**: Total gaseous mercury (TGM); co-pollutant; conditional probability function

68   (CPF); conditional bivariate probability function (CBPF); total potential source contribution

69   function (TPSCF)

70 **1. Introduction**

71   Mercury (Hg) in the atmosphere exists in three major inorganic forms including gaseous

72 elemental mercury (GEM, Hg^0), gaseous oxidized mercury (GOM, Hg^{2+}) and particulate

73 bound mercury (PBM, Hg(p)). GEM which is the dominant form of Hg in ambient air,

74 (>95%) has a relatively long residence time (0.5~2 years) due to its low reactivity and

75 solubility Schroeder and Munthe (1998). However, GOM has high water solubility and

76 relatively strong surface adhesion properties (Han et al., 2005), so it has a short atmospheric

77 residence time (~days). PBM is associated with airborne particles such as dust, soot, sea-salt

78 aerosols, and ice crystals (Lu and Schroeder, 2004) and is likely produced, in part, by

79 adsorption of GOM species such as $HgCl_2$ onto atmospheric particles (Gauchard et al., 2005;

80 Lu and Schroeder, 2004; Sakata and Marumoto, 2005; Seo et al., 2015).

81   Atmospheric Hg is emitted from both natural sources (volcanoes, volatilization from

82 aquatic and terrestrial environments) and anthropogenic sources (coal combustion, ferrous

83 and non-ferrous metals manufacturing facilities, waste incineration and industrial boilers)

84 (Lindberg et al., 2007; Pirrone et al., 2010; Schmeltz et al., 2011).

85   Atmospheric Hg released from natural and anthropogenic sources when introduced into

86 terrestrial and aquatic ecosystem through wet and dry deposition (Mason and Sheu, 2002) can

87 undergo various physical and chemical transformations before being deposited. Its lifetime in

88 the atmosphere depends on its reactivity and solubility so that depending on its form it can

89 have impacts on local, regional and global scales (Lin and Pehkonen, 1999; Lindberg et al.,

90 2007). A portion of the Hg deposited in terrestrial environments through direct industrial

91 discharge or atmospheric deposition is transported to aquatic system through groundwater

92 and surface water runoff (Miller et al., 2013).

93   A previous study also reported that Hg directly released into terrestrial and aquatic

94   ecosystems from industrial effluent has influenced surface water, sediment and biological

95   tissue (Flanders et al., 2010).

96   Significant spatial variations in atmospheric Hg deposition near urban and industrial areas

97   were due to local anthropogenic sources including municipal waste incinerators, medical

98   waste incinerators, electric power generating facilities and cement kilns (Dvonch et al.,

99   1998), ferrous and non-ferrous metal processing, iron and steel manufacturing facilities, and

100   oil and coal combustion (Hoyer et al., 1995). Miller et al. (2013) also reported that local

101   sources of elemental Hg are typically industrial processes including retort facilities used in

102   the mercury mining industry to convert Hg containing minerals to elemental Hg and chlor-

103   alkali facilities.

104   Annual anthropogenic Hg emissions in South Korea have been estimated to be 12.8 tons;

105   the major anthropogenic mercury emission sources are coal combustion in thermal power

106   plants (25.8%), oil refineries (25.5%), cement kilns (21%), incinerators (19.3%) including

107   sludge incinerators (4.7%), municipal waste incinerators (MWIs) (3%), industrial waste

108   incinerators (IWIs) (2.7%), hospital/medical/infectious waste incinerators (HMIWIs) (8.8%),

109   and iron manufacturing (7%) (Kim et al., 2010).

110   Receptor models are often used to identify sources of air pollutants and are focused on the

111   pollutants behavior in the ambient environment at the point of impact (Hopke, 2003). In

112   previous studies, conditional probability function (CPF), which utilizes the local wind

113   direction, and potential source contribution function (PSCF), which utilizes longer backward

114   trajectories (typically 3-5 days), combined with concentration data were used to identify

115   possible transport pathways and source locations (Hopke, 2003). While PSCF has been used

116   primarily to identify regional sources, it has also been used to identify local sources (Hsu et

117   al., 2003). The objectives of this study were to characterize the hourly and seasonal variations

118   of atmospheric TGM (the sum of the GEM and the GOM) concentrations, to identify the

119   relationships between TGM and co-pollutant concentrations, and to identify likely source

120   directions and locations of TGM using CPF, conditional bivariate probability function

121   (CBPF) and total PSCF (TPSCF).

122

123   **2.   Materials and methods**

124   *2.1. Sampling and analysis*

125   TGM concentrations were measured on the roof of the Korean Federation of

126   Community Credit Cooperatives (KFCCC) building (latitude: 35.992°, longitude: 129.404°,

127   ~10 m above ground) in Pohang city, in Gyeongsangbuk-do, a province in eastern South

128   Korea. Gyeongsangbuk-do has a population of 2.7 million (5% of the total population and the

129   third most populated province in South Korea) and an area of 19,030 km^2 (19% of the total

130   area of South Korea and the largest province geographically in South Korea). Pohang city has

131   a population of 500,000 (1% of the total population in South Korea) and an area of 605.4 km^2

132   (1.1% of the total area in South Korea). It is heavily industrialized with the third largest steel

133   manufacturing facility in Asia and the fifth largest in the world. There are several iron and

134   steel manufacturing facilities including electric and sintering furnaces using coking in

135   Gyeongsangbuk-do including Pohang. In addition, there are several coke plants around the

136   sampling site. The Hyungsan River divides the city into a residential area and the steel

137   complex. Hg emissions data from iron and steel manufacturing, and a hazardous waste

138   incinerator were estimated based on a previous study (Kim et al., 2010) (Fig. 1).

139   TGM concentrations were measured every 5 min during summer (17 August~23 August

140   2012), fall (9 October~17 October 2012), winter (22 January ~29 January 2013), and spring

141   (26 March~3 April 2013) using a mercury vapor analyzer (Tekran 2537B) which has two

142   gold cartridges that alternately collect and thermally desorb mercury. Ambient air at a flow

143   rate of 1.5 L min^{-1} was transported through a 3 m-long heated sampling line (1/4" OD Teflon)

144   in to the analyzer. The sampling line was heated at about 50 ºC using heat tape to prevent

145   water condensation in the gold traps because moisture on gold surfaces interferes with the

146   amalgamation of Hg (Keeler and Barres, 1999). Particulate matter was removed from the

147   sampling line by a 47 mm Teflon filter.

148

149   *2.2. Meteorological data*

150   Hourly meteorological data (air temperature, relative humidity, and wind speed and

151   direction) were obtained from the Automatic Weather Station (AWS) operated by the Korea

152   Meteorological Administration (KMA) (http://www.kma.go.kr) (6 km from the site). Hourly

153   concentrations of NO_2, O_3, CO, PM_{10} and SO_2 were obtained from the National Air Quality

154   Monitoring Network (NAQMN) (3 km from the site) (Fig. 1).

155

156   *2.3. QA/QC*

157   Automated daily calibrations were carried out for the Tekran 2537B using an internal

158   permeation source. Two-point calibrations (zero and span) were separately performed for

159   each gold cartridge. Manual injections were performed prior to every field sampling

160   campaign to evaluate these automated calibrations using a saturated mercury vapor standard.

161   The relative percent difference (RPD) between automated calibrations and manual injections

162   was less than 2%. The recovery measured by directly injecting known amounts of four

163   mercury vapor standards when the sample line was connected to zero air ranged from 92 to

164   110% (99.4 ± 5.2% in average).

165

166   **3. Model descriptions**

167   *3.1. Conditional Probability Function (CPF)*

168   CPF was originally performed to determine which wind directions dominate during high

169   concentration events to evaluate local source impacts (Ashbaugh et al., 1985). It has been

170   successfully used in many previous studies (Begum et al., 2004; Kim et al., 2003a; Kim et al.,

171   2003b; Xie and Berkowitz, 2006; Zhao et al., 2004; Zhou et al., 2004). CPF estimates the

172   probability that the measured concentration will exceed the threshold criterion for a given

173   wind direction. The CPF is defined as follows Eq. (1).

174
175    $$CPF_{\Delta\theta} = \frac{m_{\Delta\theta|c \geq x}}{n_{\Delta\theta}} \qquad (1)$$

176

177   where, $m_{\Delta\theta}$ is the number of samples from the wind sector θ having concentration C greater

178   than or equal to a threshold value *x*, and $n_{\Delta\theta}$ is the total number of samples from wind sector

179   *Δθ*. In this study, 16 sectors (Δθ = 22.5º) were used and calm winds (≤ 1 m s^{-1}) were excluded

180   from the analysis. The threshold criterion was set at above the overall average TGM

181   concentration (5.0 ng m^{-3}). Thus, CPF indicates the potential for winds from a specific

182   direction to contribute to high air pollution concentrations.

183

184   *3.2. Conditional Bivariate Probability Function (CBPF)*

185   CBPF couples ordinary CPF with wind speed as a third variable, allocating the measured

186   concentration of pollutant to cells defined by ranges of wind direction and wind speed rather

187   than to only wind direction sectors.

188   The CBPF is defined as follows Eq. (2).

189

190
$$CBPF_{\Delta\theta,\Delta u} = \frac{m_{\Delta\theta,\Delta u}|_{C \geq x}}{n_{\Delta\theta,\Delta u}} \qquad (2)$$

191

192   where, $m_{\Delta\theta,\Delta u}$ is the number of samples in the wind sector $\Delta\theta$ with wind speed interval Δu

193   having concentration C greater than a threshold value x, and $n_{\Delta\theta\Delta u}$ is the total number of

194   samples in that wind direction-speed interval. The threshold criterion was set at above the

195   overall average TGM concentration (5.0 ng m^{-3}). The extension to the bivariate case can

196   provide more information on the nature of the sources because different source types such as

197   stack emission sources and ground-level sources can have different wind speed dependencies

198   (prominent at low and high wind speed). More detailed information is described in a previous

199   study (Uria-Tellaetxe and Carslaw, 2014).

200

201   *3.3. Potential Source Contribution Function (PSCF)*

202   The PSCF model has been extensively and successfully used in the previous studies to

203   identify the likely source areas (Cheng et al., 1993; Han et al., 2004; Hopke et al., 2005; Lai

204   et al., 2007; Lim et al., 2001; Poissant, 1999; Zeng and Hopke, 1989). The PSCF is a simple

205   method that links residence time in upwind areas with high concentrations through a

206   conditional probability field and was originally developed by Ashbaugh et al. (1985). PSCF$_{ij}$

207   is the conditional probability that an air parcel that passed through the *ij*th cell had a high

208   concentration upon arrival at the monitoring site and is defined as the following Eq. (3).

209

$$PSCF_{ij} = \frac{m_{ij}}{n_{ij}} \tag{3}$$

211

212 where, n_{ij} is the number of trajectory segment endpoints that fall into the ij-th cell, and m_{ij} is the

213 number of segment endpoints in the same grid cell (ij-th cell) when the concentrations are higher

214 than a criterion value as measured at the sampling site.

215 High PSCF values in those grid cells are regarded as possible source locations. Cells including

216 emission sources can be identified with conditional probabilities close to one if trajectories that

217 have crossed the cells efficiently transport the released pollutant to the receptor site. Therefore,

218 the PSCF model provides a tool to map the source potentials of geographical areas.

219 The criterion value of PSCF for TGM concentration was set at above the overall average

220 concentration (5.0 ng m^{-3}) to identify the emission sources associated with high TGM

221 concentrations and provide a better estimation and resolution of source locations during the

222 sampling periods. The geographic area covered by the computed trajectories was divided into

223 an array of 0.05° latitude by 0.05° longitude grid cells. As will be discussed in Section 5.4, 24

224 h backward trajectories starting at every hour at a height of 10, 50, and 100 m above ground

225 level were computed using the vertical velocity model because local sources are more

226 important than that of long-range transport in this study (It should be noted that PSCF results

227 using 48 h backward trajectories had similar results as the 24 h backward trajectories). Each

228 trajectory was terminated if they exit the model top (5,000m), but advection continues along

229 the surface if trajectories intersect the ground. To generate horizontally highly resolved

230 meteorological inputs for trajectory calculations, the Weather Research and Forecast (WRF)

231 model was used to generate a coarse domain at a resolution of 27 km and a nested domain at

232 a horizontal resolution of 9 km, which geographically covers northeast Asia and the southern

233   part of the Korean Peninsula, respectively. The nested domain has 174 columns in the east-

234   west direction and 114 rows in the north-south direction. PSCF was calculated with 9 km

235   meteorological data.

236   In this study, TPSCF which incorporates probability from above different starting

237   heights was calculated since backward trajectories starting at different heights traverse

238   different distances and pathways, thus providing information that cannot be obtained from a

239   single starting height (Cheng et al., 1993).

240   Previous studies suggest that there are increasing uncertainties as backward trajectory

241   distances increase (Stohl et al., 2002) and that PSCF modeling is prone to the trailing effect is

242   which locations upwind of sources are also identified as potential sources (Han et al., 2004).

243   An alternative to back trajectory calculations in the interpretation of atmospheric trace

244   substance measurements (Stohl et al., 2002) although this technique does not provide much

245   information on source locations.

246   Generally, PSCF results show that the potential sources covered wide areas instead of

247   indicating individual sources due to the trailing effect. The trailing effect appears since PSCF

248   distributes a constant weight along the path of the trajectories. To minimize the effect of

249   small n_{ij} (the number of trajectory segment endpoints that fall into the ij-th cell) values,

250   resulting in high TPSCF values with high uncertainties, an arbitrary weight function $W(n_{ij})$

251   was applied to down-weight the PSCF values for the cell in which the total number of end

252   points was less than three times the average value of the end points (Choi et al., 2011; Heo et

253   al., 2009; Hopke et al., 1995; Polissar et al., 2001). The TPSCF value for a grid cell was

254   defined with following Eq. (4).

255

256
$$P(TPSCF_{ij}) = \frac{P(m_{ij})_{10m} + P(m_{ij})_{50m} + P(m_{ij})_{100m}}{P(n_{ij})_{10m} + P(n_{ij})_{50m} + P(n_{ij})_{100m}} \times W \qquad (4)$$

257

258   where,

259
$$W(n_{ij}) = \begin{cases} 1.0, & 3n_{ave} < n_{ij} \\ 0.8, & 2n_{ave} < n_{ij} \leq 3n_{ave} \\ 0.6, & n_{ave} < n_{ij} \leq 2n_{ave} \\ 0.4, & 0.5n_{ave} < n_{ij} \leq n_{ave} \\ 0.2, & n_{ij} \leq 0.5n_{ave} \end{cases}$$

260

4. Clean Air Policy Support System (CAPSS) data

262   In this study, the Korean National Emission Inventory estimated using Clean Air Policy

263   Support System (CAPSS) data developed by the National Institute of Environmental

264   Research (NIER) were used (http://airemiss.nier.go.kr/main.jsp (accessed December 09,

265   2015)). The CAPSS is the national emission inventory system for the air pollutants (CO,

266   NOx, SOx, TSP, PM_{10}, $PM_{2.5}$, VOCs and NH_3) which utilizes various national, regional and

267   local statistical data collected from about 150 organizations in Korea. In CAPSS, the Source

268   Classification Category (SCC) excluding fugitive dust and biomass burning based on the

269   European Environment Agency's (EEA) CORe Inventory of AIR emissions was classified

270   into the following four levels (EMEP/CORINAIR) (NIER, 2011).

271   (1) The upper level (SCC1): 11 source categories ,

272   (2) The intermediate level (SCC2): 42 source categories and

273   (3) The lower level (SCC3): 173 source categories

274

275   The sectoral contributions of emissions of South Korea, Gyeongsangbuk-do and Pohang

276   for CO, NOx, SOx, TSP, PM_{10}, $PM_{2.5}$, VOC and NH_3 are shown in Fig. S1 (See SI for

277   details).

278   More detailed information about SCCs in CAPSS is described in Table S1.

279

280   **5.   Results and Discussions**

281   *5.1. Meteorological data analysis*

282   Fig. S2 shows the frequency of counts of measured wind direction occurrence by season

283   during the sampling period. The predominant wind direction at the sampling site was W

284   (20.9%) and WS (19.2%), and calm conditions of wind speed less than 1 m s^{-1} occurred 7.6%

285   of the time. Compared to other seasons, however, the prevailing winds in summer were N

286   (17.0%), NE (16.4%), S (16.4%), and SW (15.8%).

287

288   *5.2. General characteristics of TGM*

289   The seasonal distributions of TGM were characterized by large variability during each

290   sampling period (Fig. 2). The average concentration of TGM during the complete sampling

291   period was 5.0 ± 4.7 ng m^{-3} (range: 1.0-79.6 ng m^{-3}). This is significantly higher than the

292   Northern Hemisphere background concentration (~1.5 ng m^{-3}) (Sprovieri et al., 2010) and

293   those measured in China, in Japan and other locations in Korea, however considerably lower

294   than those measured near large Hg sources in Guangzhou, China (Table 1). The median TGM

295   concentration was 3.6 ng m^{-3} which was much lower than that of the average, suggesting that

296   there were some extreme pollution episodes with very high TGM concentrations.

297   The TGM concentration follows a typical log-normal distribution (Fig. S3). The range of 2

298   to 5 ng m^{-3} dominated the distribution, accounting for more than half of the total number of

299   samples (60.8%). The maximum frequency of 28.1% occurred between 2 and 3 ng m^{-3}.

300   Extremely high TGM concentration events (>20 ng m^{-3}) were also observed (1.7% of the

301   time).

302

303   *5.3. Seasonal variations*

304   The TGM concentration was statistically significantly higher in fall (6.7 ± 6.4 ng m^{-3}) ($p <$

305   0.01), followed by spring (4.8 ± 4.0 ng m^{-3}), winter (4.5 ± 3.2 ng m^{-3}) and summer (3.8 ± 3.9

306   ng m^{-3}) (Table 2). The highest concentrations (TGM > 10 ng m^{-3}) were measured more

307   frequently in fall (24.7%), and the lowest concentrations (TGM < 3 ng m^{-3}) mainly occurred

308   in summer (49.7%). The low TGM concentration in summer is likely because increased

309   mixing height (Friedli et al., 2011), and gas phase oxidation (Choi et al., 2013; Huang et al.,

310   2010; Lynam and Keeler, 2006) at higher temperatures particularly at this sampling site

311   which is close to the ocean (2 km) where oxidation involving halogens may be enhanced

312   (Holmes et al., 2009; Lin et al., 2006). The high TGM concentrations in fall was due to

313   different wind direction (see Fig. S2), sources, relationships with other pollutants and

314   meteorological conditions. More detailed information can be found in Section 5.5.

315   The average concentrations of NO_2, O_3, CO, PM_{10} and SO_2 during the complete sampling

316   period were 23.1 ± 10.8 ppbv, 24.6 ± 12.5 ppbv, 673.7 ± 487.3 ppbv, 55.5 ± 26.4 μg m^{-3} and

317   6.7 ± 4.3 ppbv, respectively. NO_2, O_3, CO, PM_{10} and SO_2 concentrations were highest in

318   spring (Table 2). There was a statistically significant positive correlation between the TGM

319   and PM_{10} (r = 0.10) ($p < 0.01$). However, the TGM concentration was not significantly

320   correlated with NO_2, CO or SO_2 concentrations, suggesting that combustion associated with

321   space heating was not a significant source of TGM (Choi et al., 2009).

322

323   *5.4. Relationship between TGM and CO*

324   CO has a significant anthropogenic source and is considered to be an indicator of

325   anthropogenic emissions (Mao et al., 2008). Previous studies reported that TGM and CO

326   have a strong correlation because they have similar emission sources (combustion processes)

327   and similar long atmospheric residence times (Weiss-Penzias et al., 2003).

328   There was a weak positive correlation between TGM and CO in this study (r = 0.04) (p =

329   0.27). However there was a statistically significant correlation between TGM and CO in

330   winter (r = 0.25) ($p < 0.05$), suggesting that TGM and CO were affected by similar, possibly

331   distant, anthropogenic emission sources in winter.

332   On the other hand, there were no statistically significant correlations between TGM and

333   CO in spring (r = 0.02) (*p = 0.78*), in summer (r = 0.13) (*p = 0.08*), or in fall (r = -0.03) (*p =*

334   *0.69*), indicating that TGM and CO were affected by different anthropogenic emission

335   sources in these seasons.

336   Previous studies identified the long-range transport of mercury using the $\Delta TGM/\Delta CO$

337   enhancement ratio (Choi et al., 2009; Jaffe et al., 2005; Kim et al., 2009; Weiss-Penzias et al.,

338   2003; Weiss-Penzias et al., 2006). Kim et al. (2009) and Choi et al. (2009) investigated high

339   concentration events which were defined as at least a 10 h period with hourly average TGM

340   and CO concentrations higher than the average monthly TGM and CO concentrations. They

341   reported that long-range transport events were characterized by high values of TGM/CO ratio

342   ($\Delta TGM/\Delta CO$) (0.0052-0.0158 ng m^{-3} ppb^{-1}) and high correlations (r^2>0.5), whereas local

343   events showed low $\Delta TGM/\Delta CO$ (0.0005 ng m^{-3} ppb^{-1} in average) and weak correlations (r^2 <

344   0.5).

345   The observed $\Delta TGM/\Delta CO$ was 0.0001 ng m^{-3} ppb^{-1} in spring, 0.0005 ng m^{-3} ppb^{-1} in

346   summer, -0.0007 ng m^{-3} ppb^{-1} in fall, 0.0011 ng m^{-3} ppb^{-1} in winter, which are significantly

347   lower than that indicative of Asian long-range transport (0.0046-0.0056 ng m^{-3} ppb^{-1}) (Friedli

348   et al., 2004; Jaffe et al., 2005; Weiss-Penzias et al., 2006), suggesting that local sources are

349   more important than that of long-range transport in this study. The $\Delta TGM/\Delta CO$ in winter

350   (0.0011 ng m^{-3} ppb^{-1}) was similar to that of a site impacted by local sources in Korea (Kim et

351   al., 2009) and in US industrially related events (0.0011 ng m^{-3} ppb^{-1}) (Weiss-Penzias et al.,

352   2007).

353   There are also uncertainties from the potential mixing between Hg associated with long-

354   range transported airflows and local air making it difficult to distinguish between distant and

355   local source impacts. However, it is possible that the one-week sampling period in each

356   season did not capture the long-range transport events, and more can be learned using a larger

357   dataset than just using the one-week sampling period to confirm these results.

358

359   *5.5. Diurnal variations*

360   Diurnal variations of TGM (Fig. 3), co-pollutants concentrations, and meteorological

361   data were observed (Fig. S4). TGM, O_3, CO, SO_2, and temperature in the daytime (06:00-

362   18:00) were higher than those in the nighttime (18:00-06:00) ($p < 0.05$) except PM_{10} ($p =$

363   0.09) (Fig. S5). However, NO_2 during the nighttime because of relatively lower

364   photochemical reactivity with O_3 was higher than that in daytime ($p < 0.05$) (Adame et al.,

365   2012). TGM generally showed a consistent diurnal variation with an increase in the early

366   morning (06:00-09:00) and a decrease in the afternoon (14:00-17:00), similar to previous

367   studies (Dommergue et al., 2002; Friedli et al., 2011; Li et al., 2011; Liu et al., 2011; Mao et

368   al., 2008; Shon et al., 2005; Song et al., 2009; Stamenkovic et al., 2007).

369   The daytime TGM concentration (5.3 ± 4.7 ng m^{-3}) was higher than that in the nighttime

370   (4.7 ± 4.7 ng m^{-3}) ($p < 0.01$), which was similar to several previous studies (Cheng et al.,

371   2014; Gabriel et al., 2005; Nakagawa, 1995; Stamenkovic et al., 2007) but different than

372   another studies (Lee et al., 1998). Previous studies reported that this different is due to local

373   sources close to the sampling site (Cheng et al., 2014; Gabriel et al., 2005), a positive

374   correlation between TGM concentration and ambient air temperature (Nakagawa, 1995) and

375   increased traffic (Stamenkovic et al., 2007). However, another study suggested that the higher

376   TGM concentration during the night was due to the shallowing of the boundary layer, which

377   concentrated the TGM near the surface (Lee et al., 1998).

378   In a previous study the daytime TGM concentration was relatively lower than that in the

379   nighttime because the sea breeze transported air containing low amounts of TGM from the

380   ocean during the daytime whereas the land breeze transported air containing relatively high

381   concentrations of TGM from an urban area during the nighttime (Kellerhals et al., 2003).

382   Although it is possible that the land-sea breeze may affect diurnal variations in TGM

383   concentrations since the sampling site was near the ocean and lower TGM were also observed

384   during the daytime, the higher concentrations in the daytime than those in nighttime were due

385   to local emission sources because the daytime temperature (14.7 ± 10.0 ºC) was statistically

386   significantly higher than that in the nighttime (13.0 ± 9.8 ºC) (t-test, $p < 0.05$) and there was a

387   weak but statistically significant negative correlation between TGM concentration and

388   ambient air temperature (r = -0.08) ($p < 0.05$). In addition, there are several known Hg

389   sources such as iron and steel manufacturing facilities including electric and sintering

390   furnaces using coking between the sampling site and the ocean.

391   As shown in Fig. 3 and Fig. S4, there was a weak but negative relationship between the

392   TGM concentrations and O_3 concentrations (r = -0.18) ($p < 0.01$), suggesting that oxidation

393   of GEM in the oxidizing atmosphere during periods of strong atmospheric mixing was

394   partially responsible for the diurnal variations of TGM concentrations. In addition, oxidation

395   of GEM by bromine species in the coastal area (Obrist et al., 2011) or by chloride radicals in

396   marine boundary layer (Laurier et al., 2003) might play a significant role. If oxidation of

397   GEM occurred, GOM concentrations would increase. However there are uncertainties on the

398   net effects on TGM (the sum of the GEM and the GOM) since we did not measure GOM

399   concentrations.

400   Significantly different diurnal patterns have been observed at many suburban sites with

401   the daily maximum occurring in the afternoon (12:00-15:00), possibly due to local emission

402   sources and transport (Fu et al., 2010; Fu et al., 2008; Kuo et al., 2006; Wan et al., 2009).

403   Other studies in Europe reported that TGM concentrations were relatively higher early in the

404   morning or at night possibly due to mercury emissions from surface sources that accumulated

405   in the nocturnal inversion layer (Lee et al., 1998; Schmolke et al., 1999).

406   TGM concentration was negatively correlated with ambient air temperature *(r = -0.08)*

407   *(p < 0.05)* because high ambient air temperature in the daytime will increase the height of the

408   boundary layer and dilute the TGM, and the relatively lower boundary layer at nighttime

409   could concentrate the TGM in the atmosphere (Li et al., 2011). Although there was a

410   statistically significant negative correlation between the TGM concentration and ambient air

411   temperature, there was a rapid increase in TGM concentration between 06:00-09:00 when

412   ambient temperatures also increased possibly due to local emissions related to industrial

413   activities, increased traffic, and activation of local surface emission sources. Similar patterns

414   were found in previous studies (Li et al., 2011; Stamenkovic et al., 2007). Nonparametric

415   correlations revealed that there is a positive correlation between TGM and ambient air

416   temperature ($r_s = 0.11$, *p=0.27*) between 06:00-09:00. The TGM concentration was negatively

417   correlated with O_3 ($r_s = -0.33$, *p<0.01*) but positively correlated with NO_2 ($r_s = 0.21$, *p<0.05*),

418   suggesting that the increased traffic is the main source of TGM during these time periods.

419   Compared to other seasons, significantly different diurnal variations of TGM were

420   observed in fall. The daytime TGM concentrations in fall were similar to those in other

421   seasons, however, the nighttime TGM concentrations in fall were much higher than other

422   seasons. As described earlier in Section 5.3, the high TGM concentrations in fall was

423   possibly due to the relationship between other pollutants and meteorological conditions as

424   well as different wind direction and sources. The nighttime TGM concentrations in fall were

425   simultaneously positively correlated with PM_{10} (r=0.26) (*p<0.05*) and CO (r=0.21) (*p<0.05*)

426   concentrations and wind speed (r=0.35) (*p<0.01*), suggesting that the combustion process is

427   an important source during this period.

428   Based on the above results, the diurnal variations in TGM concentration are due to a

429   combination of: 1) reactions with an oxidizing atmosphere, 2) changes in ambient

430   temperature and 3) local emissions related to industrial activities. To supplement these

431   conclusions CPF and CBPF were used to identify source directions and TPSCF was used to

432   identify potential source locations.

433

434   *5.6. CPF, CBPF and TPSCF results of TGM*

435   Conventional CPF, CBPF and TPSCF plots for TGM concentrations higher than the

436   average concentration show high source probabilities to the west in the direction of large steel

437   manufacturing facilities and waste incinerators (Fig. 4). The CPF only shows high

438   probabilities from the west and provides no further information, however, the CBPF shows

439   groups of sources with the high probabilities from the west and the northeast. CBPF shows

440   that the high probabilities from the west occurred under high wind speed (> 3 m s^{-1})

441   indicative of emissions from stacks as well as low wind speed (≤ 3 m s^{-1}) indicative of non-

442   buoyant ground level sources (Uria-Tellaetxe and Carslaw, 2014).

443   As described in Section 5.4, correlations between TGM and CO revealed that TGM and

444   CO were affected by similar anthropogenic emission sources in winter but affected by

445   different sources in spring, summer and fall, which is supported by Fig. S6 which shows

446   significantly different seasonal patterns of CPF and CBPF for TGM concentrations.

447   It is difficult to discuss about the different seasonal patterns for CPF and CBPF for TGM

448   concentrations since there were no correlations between TGM and other pollutants in spring,

449   summer and fall except O_3. However, compared to Fig. 4, the CPF and CBPF patterns in fall

450   were similar to those during the whole sampling periods. Especially, the nighttime TGM

451   concentration in fall was simultaneously positively correlated with PM_{10} (r=0.26) ($p<0.05$)

452   and CO (r=0.21) ($p<0.05$) concentrations and wind speed (r=0.35) (p<0.01), indicating that

453   the combustion process from the west is an important source during this period.

454   Since TGM showed a significant correlation with CO (r=0.25) ($p<0.05$) and showed a

455   weak positive correlation with PM_{10} (r=0.08) ($p=0.33$) in winter with high wind speed,

456   combustion sources from the west are likely partially responsible for this result.

457   TPSCF identified the likely sources of TGM as the iron and manufacturing facilities and

458   the hazardous waste incinerators which are located to the west from the sampling site. A

459   previous study reported that the waste incinerators (9%) and iron and steel manufacturing

460   (7%) were relatively high Hg emissions sources in Korea (Kim et al., 2010). Waste

461   incinerators emissions were due to the high Hg content in the waste (Lee et al., 2004).

462   Emissions from iron and steel manufacturing are due to the numerous electric and sintering

463   furnaces using coking which emits relatively high mercury concentrations (Lee et al., 2004)

464   in Gyeongsangbuk-do including Pohang. There are several coke plants around the sampling

465   site (http://www.poscoenc.com/upload/W/BUSINESS/PDF/ENG_PLANT_2_1_3_5.pdf

466   (accessed December 09, 2015)). They are essential parts of the iron and steel manufacturing,

467   and the major source of atmospheric mercury related to the iron and steel manufacturing is

468   from coke production (Pacyna et al., 2006).

469   The coastal areas east of the sampling site where there are large ports were also identified

470   as the likely source areas of TGM. A previous study reported that the emissions of gaseous

471   and particulate pollutants were high during vehicular operations in port areas and from

472   marine vessel and launches (Gupta et al., 2002). Another possibility is that significant amount

473   of GEM are emitted from the ocean surface because of photo-chemically and

474   microbiologically mediated photo-reduction of dissolved GOM (Amyot et al., 1994; Zhang

475   and Lindberg, 2001). The northeast direction including the East Sea was also identified as

476   potential source areas likely because this is an area with lots of domestic passenger ships

477   routes. The south from the sampling was also identified as a likely source area of TGM where

478   Ulsan Metropolitan City, South Korea's seventh largest metropolis with a population of over

479   1.1 million is located. It includes a large petrochemical complex known as a TGM source

480   (Jen et al., 2013).

481

482   **Conclusions**

483   During the sampling periods, the average TGM concentration was higher than the Northern

484   Hemisphere background concentration, however, considerably lower than those near

485   industrial areas in China and higher than those in Japan and other locations in Korea. The

486   median concentration of TGM was much lower than that of the average, suggesting that there

487   were some extreme pollution episodes with very high TGM concentrations. The TGM

488   concentration was highest in fall, followed by spring, winter and summer. The high TGM

489   concentration in fall is due to transport from different wind directions than during the other

490   periods. The low TGM concentration in summer is likely due to increased mixing height and

491   gas phase oxidation at higher temperatures particularly at this sampling site which is close to

492   the ocean (2 km) where oxidation involving halogens may be enhanced.

493   TGM consistently showed a diurnal variation with a maximum in the early morning

494   (06:00-09:00) and minimum in the afternoon (14:00-17:00). Although there was a statistically

495   significant negative correlation between the TGM concentration and ambient air temperature,

496   the daytime TGM concentration was higher than those in the nighttime, suggesting that local

497   emission sources are important. There was a negative relationship between the TGM

498   concentrations and O_3 concentrations, indicating that the oxidation was partially responsible

499   for the diurnal variations of TGM concentrations. The observed $\Delta TGM/\Delta CO$ was

500   significantly lower than that indicative of Asian long-range transport, suggesting that local

501   sources are more important than that of long-range transport. CPF only shows high

502   probabilities to the west from the sampling site where there are large steel manufacturing

503   facilities and waste incinerators. However, CBPF and TPSCF indicated that the dominant

504   sources of TGM were the hazardous waste incinerators and the coastal areas in the northeast

505   as well as the iron and manufacturing facilities in the west. The domestic passenger ships

506   routes in the East Sea were also identified as possible source areas.

507

508   **Author contribution**

509   Yong-Seok Seo conducted a design of the study, the experiments and analysis of data, wrote

510   the initial manuscript, and finally approved the final manuscript. Seung-Pyo Jeong, Eun Ha

511   Park, Tae Young Kim, Hee-Sang Eum, Dae Gun Park, Eunhye Kim, Jaewon Choi and Jeong-

512   Hun Kim conducted the experiments, analysis of data, and finally approved the final

513   manuscript. Thomas M. Holsen, Young-Ji Han and Eunhwa Choi and Soontae Kim

514   conducted interpretation of the results, revision of the initial manuscript, and finally approved

515   the final manuscript. Seung-Muk Yi conducted a design of the study, acquisition of data of the

516   study, interpretation of data, and revision of the initial manuscript, and finally approved the final

517   manuscript.

518

519   **Acknowledgments**

520   We thank National Institute of Environmental Research (NIER) for providing CAPSS data.

521   This work was supported by Brain Korea 21 (BK21) Plus Project (Center for Healthy

522   Environment Education and Research) through the National Research Foundation (NRF) of

523   Korea and Korea Ministry of Environment (MOE) as "the Environmental Health Action

524   Program".

525

526 **Table List**

527 Table 1. Comparison with previous studies for TGM concentrations.

528 Table 2. Summary of atmospheric concentrations of TGM and co-pollutants, and

529 meteorological data.

530

531 **Figure List**

532 Fig. 1. The location of sampling site in this study ((a) South Korea, (b) Gyeongsangbuk-do

533 and (c) Pohang).

534 Fig. 2. Time-series of TGM concentrations in this study.

535 Fig. 3. The diurnal variations of TGM concentrations during the sampling periods.

536 Fig. 4. CPF, CBPF and TPSCF plots for TGM higher than average concentration.

537 **Table 1.** Comparison with previous studies for TGM concentrations.

Country	Location	Sampling period	TGM conc. (ng m^{-3})	Classifications	Reference
China	Mt. Waliguan, Qinghai–Tibet Plateau	Oct. 2007 ~ Sep. 2009	2.1	Remote	Fu et al. (2015)
China	Mt. Hengduan, Qinghai–Tibet Plateau	Jul. 2010 ~ Oct. 2010	2.5	Remote	Fu et al. (2015)
China	Nanjing, Jiangsu	Jan. 2011 ~ Oct. 2011	7.9	Urban	Hall et al. (2014)
China	Mt. Dinghu, Guangdong	Oct. 2009 ~ Apr. 2010	5.1	Rural	Chen et al. (2013)
China	Guangzhou, Guangdong	Nov. 2010 ~ Nov. 2011	4.6	Urban	Chen et al. (2013)
China	Nanjing, Jiangsu	Jan. 2011 ~ Dec. 2011	7.9	Urban	Zhu et al. (2012)
China	Guangzhou, Guangdong	Jul. 1999 ~ Jul. 2000	13.5 - 25.4	Urban	Fang et al. (2004)
China	Gui Yang, Guizhou	Jan. 2010 ~ Feb. 2010	8.4	Urban	Feng et al. (2004)
China	Changchun, Jilin	Sep. 1999 ~ Aug. 2000	9.1-15.4	Suburban	Fang et al. (2004)
Japan	Fukuoka	Jun. 2012 ~ May 2013	2.33	Urban	Marumoto et al. (2015)
Japan	Tokai-mura	Oct. 2005 ~ Aug. 2006	3.8	Suburban	Osawa et al. (2007)
Japan	Tokyo	Apr. 2000 ~ Mar. 2001	2.7	Urban	Sakata and Marumoto (2002)
Korea	Seoul	1987 ~ 2013	3.7	Urban	Kim et al. (2016)
Korea	Gangwon-do, Chuncheon	2006 ~ 2009	2.1	Rural	Han et al. (2014)
Korea	Seoul	Feb. 2005 ~ Feb. 2006	3.2	Urban	Kim et al. (2009)
Korea	Seoul	Feb. 2005 ~ Dec. 2006	3.4	Urban	Choi et al. (2009)
Korea	Seoul	19 Sep. 1997 ~ 29 Sep. 1997 27 May. 1998 ~ 18 Jun. 1998	3.6	Urban	Kim and Kim (2001)
Korea	Gyeongsangbuk-do, Pohang	17 Aug. 2012 ~ 23 Aug. 2012 9 Oct. 2012 ~ 17 Oct. 2012 22 Jan. 2013 ~ 29 Jan. 2013 26 Mar. 2013 ~ 3 Apr. 2013	5.0	Urban	This study

538

539 **Table 2.** Summary of atmospheric concentrations of TGM and co-pollutants, and meteorological data. Note that TGM was measured every 5-
540 min, and other pollutants and meteorological data were measured every 1-hour.

		TGM (ng m^{-3})	NO$_2$ (ppb)	O$_3$ (ppb)	CO (ppb)	PM$_{10}$ (μg m^{-3})	SO$_2$ (ppb)	Temperature (℃)	Wind speed (m s^{-1})	Humidity (%)	Solar radiation (MJ m^{-2})
	N	2139	189	215	215	215	215	216	216	216	216
Spring	Average	4.8 ± 4.0	25.3 ± 9.0	29.4 ± 14.2	766.5 ± 505.2	70.1 ± 26.0	7.6 ± 3.8	10.5 ± 4.2	2.2 ± 1.2	56.2 ± 16.8	0.82 ± 1.09
	Range	1.9 – 45.3	8 – 55	2 – 58	300 – 3100	28 - 204	5 - 35	1.1 – 21.6	0.4 – 6.2	19.0 – 94.0	0 – 3.44
	N	1863	187	188	187	188	188	186	180	186	141
Summer	Average	3.8 ± 3.9	18.3 ± 9.2	18.9 ± 10.1	697.3 ± 689.7	35.1 ± 15.8	6.5 ± 6.2	26.6 ± 4.2	2.2 ± 1.1	82.5 ± 13.9	0.40 ± 0.69
	Range	1.2 – 75.9	4 – 44	5 – 48	200 – 3300	12 – 87	2 - 27	19.7 – 34.1	0.1 – 6.4	43 - 98	0 – 2.92
	N	2226	212	212	212	212	211	216	216	216	216
Fall	Average	6.7 ± 6.4	25.0 ± 7.8	23.7 ± 13.1	662.7 ± 350.2	58.1 ± 17.8	5.3 ± 3.5	17.4 ± 3.2	2.1 ± 0.8	54.5 ± 14.7	0.62 ± 0.90
	Range	1.0 – 79.6	9 – 53	6 – 69	300 – 2900	20 - 145	3 - 39	11.7 – 25.2	0.5 – 4.5	12 - 79	0 – 2.90
	N	1917	188	187	188	188	186	192	192	192	192
Winter	Average	4.5 ± 3.2	23.5 ± 14.7	26.1 ± 8.7	556.4 ± 298.9	56.3 ± 30.5	7.4 ± 2.5	1.1 ± 4.3	2.8 ± 1.1	46.3 ± 24.5	0.43 ± 0.71
	Range	1.3 – 66.4	5 – 74	1 – 41	200 – 2400	18 – 161	5 – 24	-0.65 – 10.1	0.5 – 6.0	11 - 90	0 – 2.34
	N	8145	776	802	802	803	800	810	804	810	765
Total	Average	5.0 ± 4.7	23.1 ± 10.8	24.6 ± 12.5	673.7 ± 487.3	55.5 ± 26.4	6.7 ± 4.3	13.8 ± 9.9	2.3 ± 1.1	59.4 ± 22.1	0.59 ± 0.90
	Range	1.0 – 79.6	4 – 74	1 – 69	200 – 3300	12 – 204	2 – 39	-6.5 – 34.1	0.1 – 6.4	11 - 98	0 – 3.44

541

542
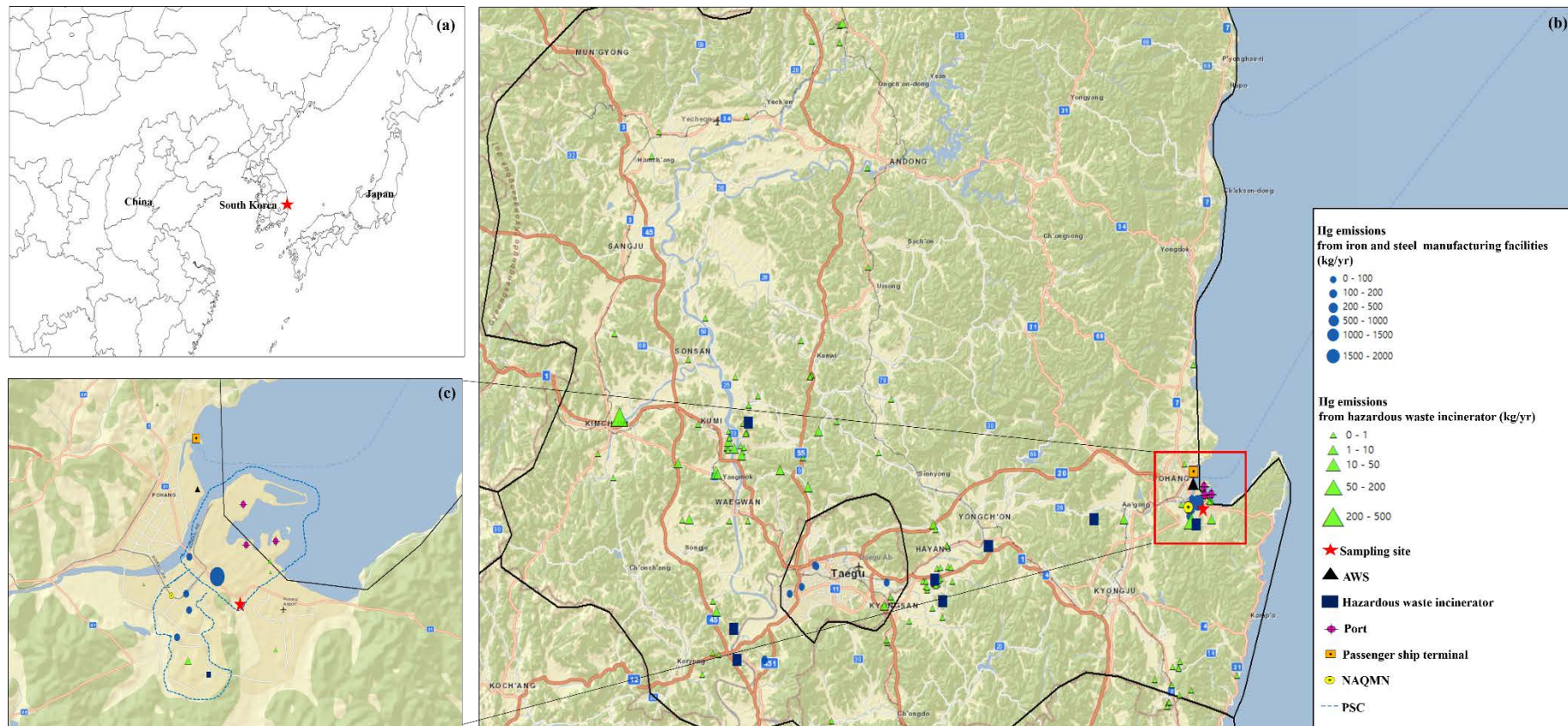
Fig. 1. The location of sampling site in this study ((a) South Korea, (b) Gyeongsangbuk-do and (c) Pohang). AWS, NAQMN and PSC represent Automatic Weather Station, National Air Quality Monitoring Network and Pohang Steel Complex, respectively.
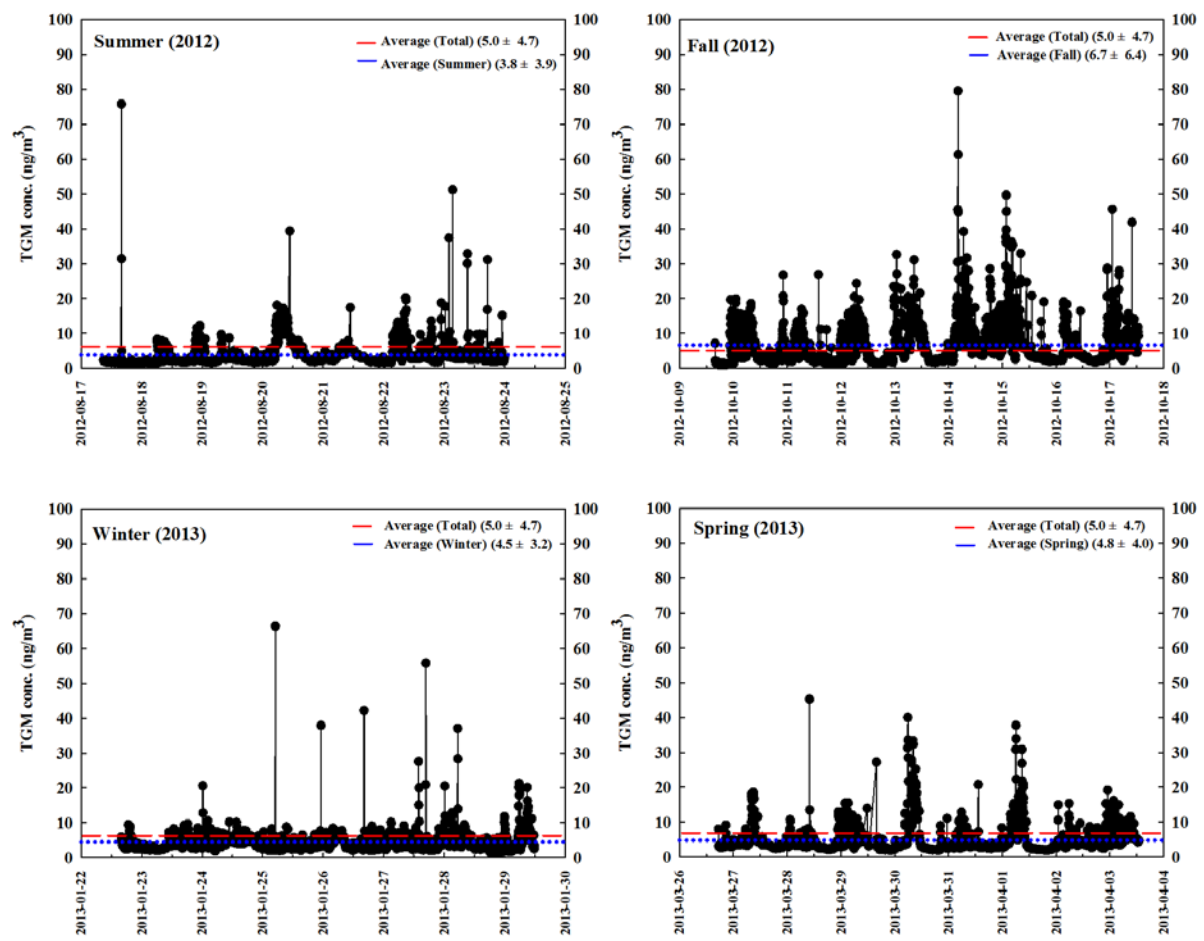
543

544   **Fig. 2.** Time-series of TGM concentrations in this study.
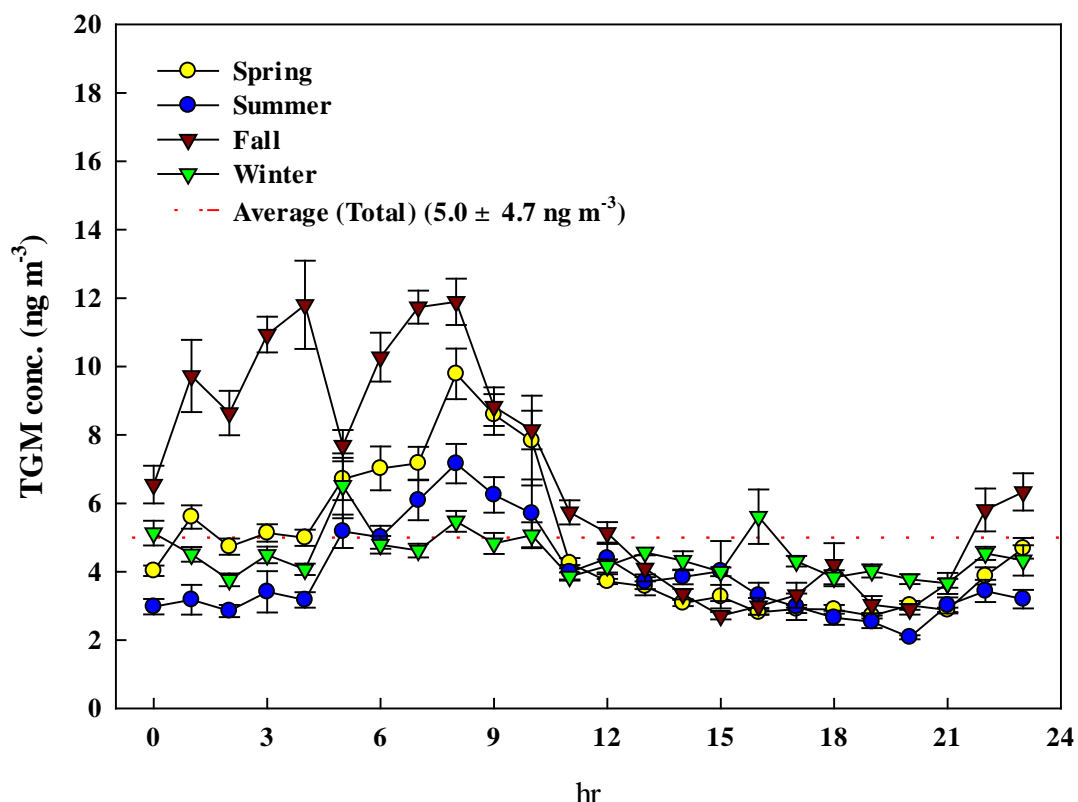
545
546 **Fig. 3.** The diurnal variations of TGM concentrations during the sampling periods.
547 The error bars represent standard error.
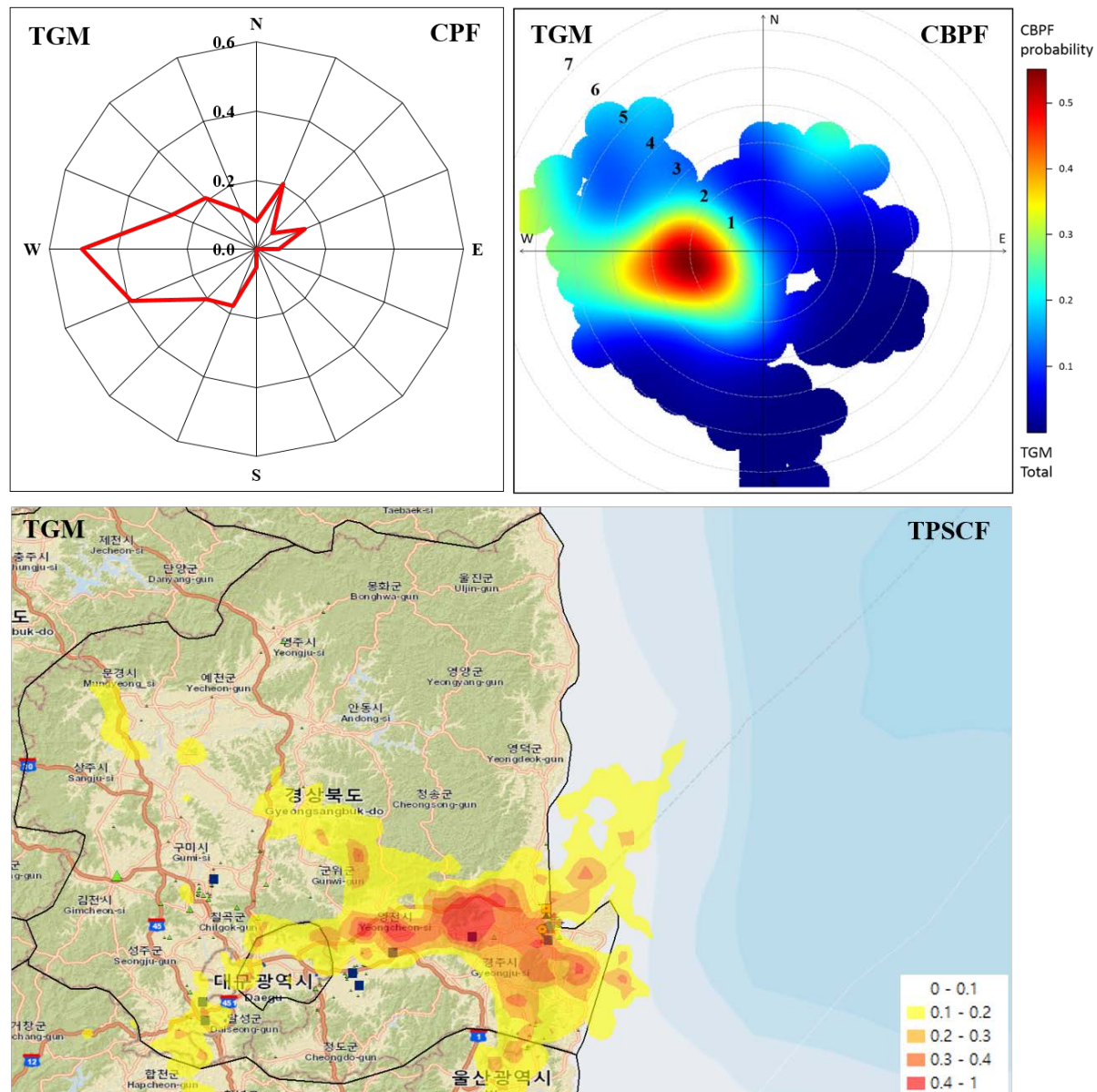
548
549
550 **Fig. 4.** CPF, CBPF and TPSCF plots for TGM higher than average concentration. The radial
551 axes of CPF and CBPF are the probability and the wind speed (m s^{-1}), respectively.

References

Adame, J., Notario, A., Villanueva, F. and Albaladejo, J.: Application of cluster analysis to surface ozone, NO$_2$ and SO$_2$ daily patterns in an industrial area in Central-Southern Spain measured with a DOAS system. Sci. Total Environ., 429, 281-291. 2012.

Amyot, M., McQueen, D. J., Mierle, G. and Lean, D. R.: Sunlight-induced formation of dissolved gaseous mercury in lake waters. Environ. Sci. Technol., 28, 2366-2371. 1994.

Ashbaugh, L. L., Malm, W. C. and Sadeh, W. Z.: A residence time probability analysis of sulfur concentrations at Grand Canyon National Park. Atmospheric Environment (1967), 19, 1263-1270. 1985.

Begum, B. A., Kim, E., Biswas, S. K. and Hopke, P. K.: Investigation of sources of atmospheric aerosol at urban and semi-urban areas in Bangladesh. Atmos. Environ., 38, 3025-3038. 2004.

Chen, L., Liu, M., Xu, Z., Fan, R., Tao, J., Chen, D., Zhang, D., Xie, D. and Sun, J.: Variation trends and influencing factors of total gaseous mercury in the Pearl River Delta—A highly industrialised region in South China influenced by seasonal monsoons. Atmos. Environ., 77, 757-766. 2013.

Cheng, I., Zhang, L., Mao, H., Blanchard, P., Tordon, R. and Dalziel, J.: Seasonal and diurnal patterns of speciated atmospheric mercury at a coastal-rural and a coastal-urban site. Atmos. Environ., 82, 193-205. 2014.

Cheng, M. D., Hopke, P. K. and Zeng, Y.: A receptor-oriented methodology for determining source regions of particulate sulfate observed at Dorset, Ontario. Journal of Geophysical Research: Atmospheres (1984–2012), 98, 16839-16849. 1993.

Choi, E.-M., Kim, S.-H., Holsen, T. M. and Yi, S.-M.: Total gaseous concentrations in mercury in Seoul, Korea: local sources compared to long-range transport from China and Japan. Environ. Pollut., 157, 816-822. 2009.

Choi, E., Heo, J.-B., Hopke, P. K., Jin, B.-B. and Yi, S.-M.: Identification, apportionment, and photochemical reactivity of non-methane hydrocarbon sources in Busan, Korea. Water, Air, Soil Pollut., 215, 67-82. 2011.

Choi, H.-D., Huang, J., Mondal, S. and Holsen, T. M.: Variation in concentrations of three mercury (Hg) forms at a rural and a suburban site in New York State. Sci. Total Environ., 448, 96-106. 2013.

Dommergue, A., Ferrari, C. P., Planchon, F. A. and Boutron, C. F.: Influence of anthropogenic sources on total gaseous mercury variability in Grenoble suburban air (France). Sci. Total Environ., 297, 203-213. 2002.

Dvonch, J., Graney, J., Marsik, F., Keeler, G. and Stevens, R.: An investigation of source–receptor relationships for mercury in south Florida using event precipitation data. Sci. Total Environ., 213, 95-108. 1998.

Fang, F., Wang, Q. and Li, J.: Urban environmental mercury in Changchun, a metropolitan city in Northeastern China: source, cycle, and fate. Sci. Total Environ., 330, 159-170. 2004.

Feng, X., Shang, L., Wang, S., Tang, S. and Zheng, W.: Temporal variation of total gaseous mercury in the air of Guiyang, China. Journal of Geophysical Research: Atmospheres (1984–2012), 109. 2004.

Flanders, J., Turner, R., Morrison, T., Jensen, R., Pizzuto, J., Skalak, K. and Stahl, R.: Distribution, behavior, and transport of inorganic and methylmercury in a high gradient stream. Appl. Geochem., 25, 1756-1769. 2010.

600 Friedli, H., Arellano Jr, A., Geng, F., Cai, C. and Pan, L.: Measurements of atmospheric
601   mercury in Shanghai during September 2009. Atmos. Chem. Phys., 11, 3781-3788.
602   2011.
603 Friedli, H. R., Radke, L. F., Prescott, R., Li, P., Woo, J. H. and Carmichael, G. R.: Mercury in
604   the atmosphere around Japan, Korea, and China as observed during the 2001 ACE-
605   Asia field campaign: Measurements, distributions, sources, and implications. Journal
606   of Geophysical Research: Atmospheres (1984–2012), 109. 2004.
607 Fu, X., Feng, X., Dong, Z., Yin, R., Wang, J., Yang, Z. and Zhang, H.: Atmospheric gaseous
608   elemental mercury (GEM) concentrations and mercury depositions at a high-altitude
609   mountain peak in south China. Atmos. Chem. Phys., 10, 2425-2437. 2010.
610 Fu, X., Feng, X., Zhu, W., Wang, S. and Lu, J.: Total gaseous mercury concentrations in
611   ambient air in the eastern slope of Mt. Gongga, South-Eastern fringe of the Tibetan
612   plateau, China. Atmos. Environ., 42, 970-979. 2008.
613 Fu, X., Zhang, H., Lin, C.-J., Feng, X., Zhou, L. and Fang, S.: Correlation slopes of
614   GEM/CO, GEM/CO 2, and GEM/CH 4 and estimated mercury emissions in China,
615   South Asia, the Indochinese Peninsula, and Central Asia derived from observations in
616   northwestern and southwestern China. Atmos. Chem. Phys., 15, 1013-1028. 2015.
617 Gabriel, M. C., Williamson, D. G., Brooks, S. and Lindberg, S.: Atmospheric speciation of
618   mercury in two contrasting Southeastern US airsheds. Atmos. Environ., 39, 4947-
619   4958. 2005.
620 Gauchard, P.-A., Ferrari, C. P., Dommergue, A., Poissant, L., Pilote, M., Guehenneux, G.,
621   Boutron, C. F. and Baussand, P.: Atmospheric particle evolution during a nighttime
622   atmospheric mercury depletion event in sub-Arctic at Kuujjuarapik/Whapmagoostui,
623   Quebec, Canada. Sci. Total Environ., 336, 215-224. 2005.
624 Gupta, A., Patil, R. and Gupta, S.: Emissions of gaseous and particulate pollutants in a port
625   and harbour region in India. Environ. Monit. Assess., 80, 187-205. 2002.
626 Hall, C. B., Mao, H., Ye, Z., Talbot, R., Ding, A., Zhang, Y., Zhu, J., Wang, T., Lin, C.-J.
627   and Fu, C.: Sources and Dynamic Processes Controlling Background and Peak
628   Concentrations of TGM in Nanjing, China. Atmosphere, 5, 124-155. 2014.
629 Han, Y.-J., Holsen, T. M., Hopke, P. K., Cheong, J.-P., Kim, H. and Yi, S.-M.: Identification
630   of source locations for atmospheric dry deposition of heavy metals during yellow-
631   sand events in Seoul, Korea in 1998 using hybrid receptor models. Atmos. Environ.,
632   38, 5353-5361. 2004.
633 Han, Y.-J., Holsen, T. M., Hopke, P. K. and Yi, S.-M.: Comparison between back-trajectory
634   based modeling and Lagrangian backward dispersion modeling for locating sources of
635   reactive gaseous mercury. Environ. Sci. Technol., 39, 1715-1723. 2005.
636 Han, Y.-J., Kim, J.-E., Kim, P.-R., Kim, W.-J., Yi, S.-M., Seo, Y.-S. and Kim, S.-H.: General
637   trends of atmospheric mercury concentrations in urban and rural areas in Korea and
638   characteristics of high-concentration events. Atmos. Environ., 94, 754-764. 2014.
639 Heo, J.-B., Hopke, P. and Yi, S.-M.: Source apportionment of $PM_{2.5}$ in Seoul, Korea. Atmos.
640   Chem. Phys., 9, 4957-4971. 2009.
641 Holmes, C. D., Jacob, D. J., Mason, R. P. and Jaffe, D. A.: Sources and deposition of reactive
642   gaseous mercury in the marine atmosphere. Atmos. Environ., 43, 2278-2285. 2009.
643 Hopke, P., Barrie, L., Li, S. M., Cheng, M. D., Li, C. and Xie, Y.: Possible sources and
644   preferred pathways for biogenic and non-sea-salt sulfur for the high Arctic. Journal of
645   Geophysical Research: Atmospheres (1984–2012), 100, 16595-16603. 1995.
646 Hopke, P. K.: Recent developments in receptor modeling. J. Chemometrics, 17, 255-265.
647   2003.

648   Hopke, P. K., Zhou, L. and Poirot, R. L.: Reconciling trajectory ensemble receptor model
649   results with emissions. Environ. Sci. Technol., 39, 7980-7983. 2005.
650   Hoyer, M., Burke, J. and Keeler, G. 1995. Atmospheric sources, transport and deposition of
651   mercury in Michigan: two years of event precipitation. *Mercury as a Global*
652   *Pollutant.* Springer.
653   Hsu, Y.-K., Holsen, T. M. and Hopke, P. K.: Comparison of hybrid receptor models to locate
654   PCB sources in Chicago. Atmos. Environ., 37, 545-562. 2003.
655   Huang, J., Choi, H.-D., Hopke, P. K. and Holsen, T. M.: Ambient mercury sources in
656   Rochester, NY: results from principle components analysis (PCA) of mercury
657   monitoring network data. Environ. Sci. Technol., 44, 8441-8445. 2010.
658   Jaffe, D., Prestbo, E., Swartzendruber, P., Weiss-Penzias, P., Kato, S., Takami, A.,
659   Hatakeyama, S. and Kajii, Y.: Export of atmospheric mercury from Asia. Atmos.
660   Environ., 39, 3029-3038. 2005.
661   Jen, Y.-H., Yuan, C.-S., Hung, C.-H., Ie, I.-R. and Tsai, C.-M.: Tempospatial variation and
662   partition of atmospheric mercury during wet and dry seasons at sensitivity sites within
663   a heavily polluted industrial city. Aerosol Air Qual. Res, 13, 13-23. 2013.
664   Keeler, G. and Barres, J.: Sampling and Analysis for Atmospheric Mercury. Center for
665   Environmental Research Information, Cincinati. 1999.
666   Kellerhals, M., Beauchamp, S., Belzer, W., Blanchard, P., Froude, F., Harvey, B., McDonald,
667   K., Pilote, M., Poissant, L. and Puckett, K.: Temporal and spatial variability of total
668   gaseous mercury in Canada: results from the Canadian Atmospheric Mercury
669   Measurement Network (CAMNet). Atmos. Environ., 37, 1003-1011. 2003.
670   Kim, E., Hopke, P. K. and Edgerton, E. S.: Source identification of Atlanta aerosol by
671   positive matrix factorization. J. Air Waste Manage. Assoc., 53, 731-739. 2003a.
672   Kim, E., Larson, T. V., Hopke, P. K., Slaughter, C., Sheppard, L. E. and Claiborn, C.: Source
673   identification of $PM_{2.5}$ in an arid Northwest US City by positive matrix factorization.
674   Atmospheric Research, 66, 291-305. 2003b.
675   Kim, J.-H., Park, J.-M., Lee, S.-B., Pudasainee, D. and Seo, Y.-C.: Anthropogenic mercury
676   emission inventory with emission factors and total emission in Korea. Atmos.
677   Environ., 44, 2714-2721. 2010.
678   Kim, K.-H., Brown, R. J., Kwon, E., Kim, I.-S. and Sohn, J.-R.: Atmospheric mercury at an
679   urban station in Korea across three decades. Atmos. Environ., 131, 124-132. 2016.
680   Kim, K.-H. and Kim, M.-Y.: Some insights into short-term variability of total gaseous
681   mercury in urban air. Atmos. Environ., 35, 49-59. 2001.
682   Kim, S.-H., Han, Y.-J., Holsen, T. M. and Yi, S.-M.: Characteristics of atmospheric speciated
683   mercury concentrations (TGM, Hg (II) and Hg (p)) in Seoul, Korea. Atmos. Environ.,
684   43, 3267-3274. 2009.
685   Kuo, T.-H., Chang, C.-F., Urba, A. and Kvietkus, K.: Atmospheric gaseous mercury in
686   Northern Taiwan. Sci. Total Environ., 368, 10-18. 2006.
687   Lai, S.-O., Holsen, T. M., Hopke, P. K. and Liu, P.: Wet deposition of mercury at a New
688   York state rural site: concentrations, fluxes, and source areas. Atmos. Environ., 41,
689   4337-4348. 2007.
690   Laurier, F. J., Mason, R. P., Whalin, L. and Kato, S.: Reactive gaseous mercury formation in
691   the North Pacific Ocean's marine boundary layer: A potential role of halogen
692   chemistry. Journal of Geophysical Research: Atmospheres (1984–2012), 108. 2003.
693   Lee, D. S., Dollard, G. J. and Pepler, S.: Gas-phase mercury in the atmosphere of the United
694   Kingdom. Atmos. Environ., 32, 855-864. 1998.

695 Lee, S. J., Seo, Y.-C., Jurng, J., Hong, J.-H., Park, J.-W., Hyun, J. E. and Lee, T. G.: Mercury
696   emissions from selected stationary combustion sources in Korea. Sci. Total Environ.,
697   325, 155-161. 2004.
698 Li, Z., Xia, C., Wang, X., Xiang, Y. and Xie, Z.: Total gaseous mercury in Pearl River Delta
699   region, China during 2008 winter period. Atmos. Environ., 45, 834-838. 2011.
700 Lim, C.-J., Cheng, M.-D. and Schroeder, W. H.: Transport patterns and potential sources of
701   total gaseous mercury measured in Canadian high Arctic in 1995. Atmos. Environ.,
702   35, 1141-1154. 2001.
703 Lin, C.-J. and Pehkonen, S. O.: The chemistry of atmospheric mercury: a review. Atmos.
704   Environ., 33, 2067-2079. 1999.
705 Lin, C.-J., Pongprueksa, P., Lindberg, S. E., Pehkonen, S. O., Byun, D. and Jang, C.:
706   Scientific uncertainties in atmospheric mercury models I: Model science evaluation.
707   Atmos. Environ., 40, 2911-2928. 2006.
708 Lindberg, S., Bullock, R., Ebinghaus, R., Engstrom, D., Feng, X., Fitzgerald, W., Pirrone, N.,
709   Prestbo, E. and Seigneur, C.: A synthesis of progress and uncertainties in attributing
710   the sources of mercury in deposition. AMBIO: A Journal of the Human Environment,
711   36, 19-33. 2007.
712 Liu, N., Qiu, G., Landis, M. S., Feng, X., Fu, X. and Shang, L.: Atmospheric mercury species
713   measured in Guiyang, Guizhou province, southwest China. Atmospheric Research,
714   100, 93-102. 2011.
715 Lu, J. Y. and Schroeder, W. H.: Annual time-series of total filterable atmospheric mercury
716   concentrations in the Arctic. Tellus B, 56, 213-222. 2004.
717 Lynam, M. M. and Keeler, G. J.: Source–receptor relationships for atmospheric mercury in
718   urban Detroit, Michigan. Atmos. Environ., 40, 3144-3155. 2006.
719 Mao, H., Talbot, R., Sigler, J., Sive, B. and Hegarty, J.: Seasonal and diurnal variations of Hg
720   over New England. Atmos. Chem. Phys., 8, 1403-1421. 2008.
721 Marumoto, K., Hayashi, M. and Takami, A.: Atmospheric mercury concentrations at two
722   sites in the Kyushu Islands, Japan, and evidence of long-range transport from East
723   Asia. Atmos. Environ., 117, 147-155. 2015.
724 Mason, R. P. and Sheu, G. R.: Role of the ocean in the global mercury cycle. Global
725   biogeochemical cycles, 16, 40-1-40-14. 2002.
726 Miller, C. L., Watson, D. B., Lester, B. P., Lowe, K. A., Pierce, E. M. and Liang, L.:
727   Characterization of soils from an industrial complex contaminated with elemental
728   mercury. Environ. Res., 125, 20-29. 2013.
729 Nakagawa, R.: Studies on the levels in atmospheric concentrations of mercury in Japan.
730   Chemosphere, 31, 2669-2676. 1995.
731 NIER: National Air Pollutants Emission 2011 (in Korean). 2011.
732 Obrist, D., Tas, E., Peleg, M., Matveev, V., Faïn, X., Asaf, D. and Luria, M.: Bromine-
733   induced oxidation of mercury in the mid-latitude atmosphere. Nature Geoscience, 4,
734   22-26. 2011.
735 Osawa, T., Ueno, T. and Fu, F.: Sequential variation of atmospheric mercury in Tokai-mura,
736   seaside area of eastern central Japan. Journal of Geophysical Research: Atmospheres
737   (1984–2012), 112. 2007.
738 Pacyna, E. G., Pacyna, J. M., Steenhuisen, F. and Wilson, S.: Global anthropogenic mercury
739   emission inventory for 2000. Atmos. Environ., 40, 4048-4063. 2006.
740 Pirrone, N., Cinnirella, S., Feng, X., Finkelman, R., Friedli, H., Leaner, J., Mason, R.,
741   Mukherjee, A., Stracher, G. and Streets, D.: Global mercury emissions to the
742   atmosphere from anthropogenic and natural sources. Atmospheric Chemistry and
743   Physics, 10, 5951-5964. 2010.

744 Poissant, L.: Potential sources of atmospheric total gaseous mercury in the St. Lawrence
745   River valley. Atmos. Environ.*, 33*, 2537-2547. 1999.
746 Polissar, A. V., Hopke, P. K. and Harris, J. M.: Source regions for atmospheric aerosol
747   measured at Barrow, Alaska. Environ. Sci. Technol.*, 35*, 4214-4226. 2001.
748 Sakata, M. and Marumoto, K.: Formation of atmospheric particulate mercury in the Tokyo
749   metropolitan area. Atmos. Environ.*, 36*, 239-246. 2002.
750 Sakata, M. and Marumoto, K.: Wet and dry deposition fluxes of mercury in Japan. Atmos.
751   Environ.*, 39*, 3139-3146. 2005.
752 Schmeltz, D., Evers, D. C., Driscoll, C. T., Artz, R., Cohen, M., Gay, D., Haeuber, R.,
753   Krabbenhoft, D. P., Mason, R. and Morris, K.: MercNet: a national monitoring
754   network to assess responses to changing mercury emissions in the United States.
755   Ecotoxicology*, 20*, 1713-1725. 2011.
756 Schmolke, S. R., Schroeder, W., Kock, H., Schneeberger, D., Munthe, J. and Ebinghaus, R.:
757   Simultaneous measurements of total gaseous mercury at four sites on a 800km
758   transect: spatial distribution and short-time variability of total gaseous mercury over
759   central Europe. Atmos. Environ.*, 33*, 1725-1733. 1999.
760 Schroeder, W. H. and Munthe, J.: Atmospheric mercury—an overview. Atmos. Environ.*, 32*,
761   809-822. 1998.
762 Seo, Y.-S., Han, Y.-J., Holsen, T. M., Choi, E., Zoh, K.-D. and Yi, S.-M.: Source
763   identification of total mercury (TM) wet deposition using a Lagrangian particle
764   dispersion model (LPDM). Atmos. Environ.*, 104*, 102-111. 2015.
765 Shon, Z.-H., Kim, K.-H., Kim, M.-Y. and Lee, M.: Modeling study of reactive gaseous
766   mercury in the urban air. Atmos. Environ.*, 39*, 749-761. 2005.
767 Song, X., Cheng, I. and Lu, J.: Annual atmospheric mercury species in downtown Toronto,
768   Canada. J. Environ. Monit.*, 11*, 660-669. 2009.
769 Sprovieri, F., Pirrone, N., Ebinghaus, R., Kock, H. and Dommergue, A.: A review of
770   worldwide atmospheric mercury measurements. Atmos. Chem. Phys.*, 10*, 8245-8265.
771   2010.
772 Stamenkovic, J., Lyman, S. and Gustin, M. S.: Seasonal and diel variation of atmospheric
773   mercury concentrations in the Reno (Nevada, USA) airshed. Atmos. Environ.*, 41*,
774   6662-6672. 2007.
775 Stohl, A., Eckhardt, S., Forster, C., James, P., Spichtinger, N. and Seibert, P.: A replacement
776   for simple back trajectory calculations in the interpretation of atmospheric trace
777   substance measurements. Atmos. Environ.*, 36*, 4635-4648. 2002.
778 Uria-Tellaetxe, I. and Carslaw, D. C.: Conditional bivariate probability function for source
779   identification. Environ. Model. Software*, 59*, 1-9. 2014.
780 Wan, Q., Feng, X., Lu, J., Zheng, W., Song, X., Han, S. and Xu, H.: Atmospheric mercury in
781   Changbai Mountain area, northeastern China I. The seasonal distribution pattern of
782   total gaseous mercury and its potential sources. Environ. Res.*, 109*, 201-206. 2009.
783 Weiss-Penzias, P., Jaffe, D., Swartzendruber, P., Hafner, W., Chand, D. and Prestbo, E.:
784   Quantifying Asian and biomass burning sources of mercury using the Hg/CO ratio in
785   pollution plumes observed at the Mount Bachelor Observatory. Atmos. Environ.*, 41*,
786   4366-4379. 2007.
787 Weiss-Penzias, P., Jaffe, D. A., McClintick, A., Prestbo, E. M. and Landis, M. S.: Gaseous
788   elemental mercury in the marine boundary layer: Evidence for rapid removal in
789   anthropogenic pollution. Environ. Sci. Technol.*, 37*, 3755-3763. 2003.
790 Weiss-Penzias, P., Jaffe, D. A., Swartzendruber, P., Dennison, J. B., Chand, D., Hafner, W.
791   and Prestbo, E.: Observations of Asian air pollution in the free troposphere at Mount

792   Bachelor Observatory during the spring of 2004. Journal of Geophysical Research:
793   Atmospheres (1984–2012), 111. 2006.
794 Xie, Y. and Berkowitz, C. M.: The use of positive matrix factorization with conditional
795   probability functions in air quality studies: an application to hydrocarbon emissions in
796   Houston, Texas. Atmos. Environ., 40, 3070-3091. 2006.
797 Zeng, Y. and Hopke, P.: A study of the sources of acid precipitation in Ontario, Canada.
798   Atmospheric Environment (1967), 23, 1499-1509. 1989.
799 Zhang, H. and Lindberg, S. E.: Sunlight and iron (III)-induced photochemical production of
800   dissolved gaseous mercury in freshwater. Environ. Sci. Technol., 35, 928-935. 2001.
801 Zhao, W., Hopke, P. K. and Karl, T.: Source identification of volatile organic compounds in
802   Houston, Texas. Environ. Sci. Technol., 38, 1338-1347. 2004.
803 Zhou, L., Kim, E., Hopke, P. K., Stanier, C. O. and Pandis, S.: Advanced factor analysis on
804   Pittsburgh particle size-distribution data special issue of aerosol science and
805   technology on findings from the Fine Particulate Matter Supersites Program. Aerosol
806   Science and Technology, 38, 118-132. 2004.
807 Zhu, J., Wang, T., Talbot, R., Mao, H., Hall, C., Yang, X., Fu, C., Zhuang, B., Li, S. and Han,
808   Y.: Characteristics of atmospheric total gaseous mercury (TGM) observed in urban
809   Nanjing, China. Atmos. Chem. Phys., 12, 12103-12118. 2012.